Colloids and Surfaces A 560 (2019) 352–359

Contents lists available at ScienceDirect

Colloids and Surfaces A

journal homepage: www.elsevier.com/locate/colsurfa

Bioinspired multifunctional polymer–nanoparticle–surfactant complex nanocomposite surfaces for antibacterial oil–water separation

A.W. Ritchie[a], H.J. Cox[a], S.N. Barrientos-Palomo[a], G.J. Sharples[b], J.P.S. Badyal[a,*]

[a] Chemistry Department, Durham University, Durham DH1 3LE, England, UK
[b] Department of Biosciences, Durham University, Durham DH1 3LE, England, UK

GRAPHICAL ABSTRACT

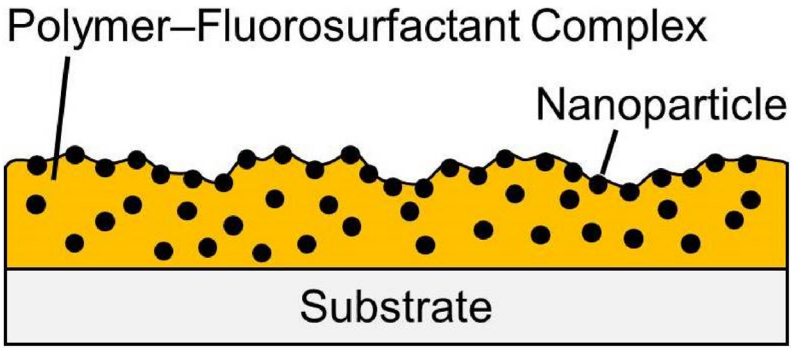

ARTICLE INFO

Keywords:
Polymer–nanoparticle–fluorosurfactant complex
Oleophobic–hydrophilic
Antibacterial
Oil–water separation
Anti-fogging

ABSTRACT

Bioinspired polymer–nanoparticle–fluorosurfactant complex composite coatings are shown to display fast-switching oleophobic–hydrophilic properties. The large switching parameters (difference between the equilibrium oil and water static contact angles) are attributed to nanoparticle enhanced surface roughening (leading to improvement in hydrophilicity and oleophobicity for optimum nanoparticle loadings). Nanoparticle incorporation also increases hardness of the coatings (durability). Porous substrates coated with these polymer–nanoparticle–fluorosurfactant complex composite coatings are found to readily separate oil–water mixtures under both static and continuous flow as well as displaying antibacterial surface properties against *Escherichia coli* (Gram-negative bacteria) and *Staphylococcus aureus* (Gram-positive bacteria). A key advantage of this approach for coating substrates is its single-step simplicity. Potential applications include provision of safe drinking water, environmental pollution clean-up, and anti-fogging.

1. Introduction

Oil-spill clean-up is an important environmental challenge due to the significant long-term effects such accidents have on oceans and aquatic species [1–6]. Absorbent materials are reported to remove oil from oil–water mixtures—however, these materials need additional steps to remove the absorbed oil and to regenerate the material for re-use; and water absorption during oil recovery reduces their efficiency (unsuitable for continuous oil–water separation processes) [7–13]. Separation membranes which have opposing wetting properties towards water versus oil can be utilised for continuous oil–water mixture separation [14–21]. Due to the relative surface energies of typical oils

* Corresponding author.
E-mail address: j.p.badyal@durham.ac.uk (J.P.S. Badyal).

https://doi.org/10.1016/j.colsurfa.2018.10.030
Received 12 August 2018; Received in revised form 10 October 2018; Accepted 10 October 2018
Available online 11 October 2018

(20–30 mN m^{-1}) versus water (72 mN m^{-1}), conventional membranes repel water while allowing oil to pass through [22–24]. However, these oleophilic–hydrophobic materials are easily fouled by oils causing blockage and a drop in efficiency. Furthermore, the greater density of water compared to oils can lead to the formation of a surface water layer which blocks the passage of oil [25]. Simply by reversing the wettability, these drawbacks can be overcome (oleophobic–hydrophilic surfaces repel oil but are wetted by water). Oils are repelled and so do not easily foul the surface, while the hydrophilic nature of such materials helps to remove any contaminants in contact with the surface [26]. The main disadvantage of such oleophobic–hydrophilic surfaces has been the complexity of their preparation and methods of application. One approach for oleophobic–hydrophilic surfaces has been the use of superhydrophilic surfaces—when underwater, the water layer formation on the surface helps to repel oils providing an underwater oleophobic surface [27–29]. The major disadvantage of these underwater oleophobic–hydrophilic systems is that the filter must constantly be kept in a wetted state (as soon as the filter dries up the oil will pass through) [30]. They are also easily contaminated by oils due to their in-air oleophilic properties. Therefore, surfaces which display both in-air oleophobicity and hydrophilicity are more desirable for oil–water separation applications. In addition, these are also suitable for other uses such as anti-fogging [26,31–33] and self-cleaning [26,31,32].

One way to fabricate oleophobic–hydrophilic surfaces is to utilise polymer–fluorosurfactant complexes (the fluorosurfactant complexes to the polymer backbone through electrostatic interaction) [34–37]. These surfaces can be prepared either by a multi-step layer-by-layer approach [38,39] or by direct application of the polymer–fluorosurfactant complex onto the substrate [40–42]. For both cases, the oil repellency of the polymer–fluorosurfactant coating stems from the low-surface-energy fluorinated tail of the fluorosurfactant being orientated towards the air–solid interface [43]. This localises the hydrophilic fluorosurfactant head groups in the sub-surface region where they are complexed to the hydrophilic groups of the polymer. When water molecules are placed onto the surface, they wick down towards the hydrophilic subsurface resulting in surface wetting [44]. It has been suggested that this happens through defects in the fluorinated layer, whilst oil molecules are too large to penetrate them [45,46]. Another possible mechanism is water-induced surface rearrangement of the fluorinated chains allowing penetration of the water molecules; whilst in the presence of oils, this rearrangement does not take place, and so the top-most low-surface-energy fluorinated chains repel oil [47].

Early reports of polymer–fluorosurfactant coated surfaces showed little difference between the oil and water contact angles [34,37,43,48]. Improvements in hydrophilicity were subsequently achieved through the utilisation of plasma polymer–fluorosurfactant coatings leading to larger switching parameters (the difference in the static hexadecane and water contact angles)—however, this remained a two-step process [49–51]. Although single-step processes have been reported, these surfaces tend to be initially hydrophobic, and it can take several minutes for them to achieve their final hydrophilic state [40,41]. One notable exception has been fast-switching copolymer–fluorosurfactant surfaces where water wets within 10 s whilst oleophobicity is retained [42]. This oil repellency was improved further through the use of solvent-induced roughening to yield switching parameters in the order of 100°. A comparable switching parameter (90–95°) has been reported by adding nanoparticles to the polymer–fluorosurfactant complex solution mixture—however, oil–water separation experiments take several minutes to allow the water to pass through due to the requirement for very small aperture meshes (~42 to 60 μm), therefore this system is not suitable for continuous oil–water separation [47]. Although good initial oil repellency and hydrophilicity have been reported for a layer-by-layer approach where the polymer, fluorosurfactant, and silica nanoparticles are deposited in sequential steps—this is a lengthy process and not well suited to industrial scale-up [39,52].

In this study, nanocomposite oleophobic–hydrophilic surfaces have been deposited in a single step by using polymer–nanoparticle–-fluorosurfactant complexes which display a marked enhancement in the switching parameter. Coating of large aperture (310 μm) meshes provides for high efficiency continuous oil–water separation performance, Scheme 1. The incorporation of nanoparticles improves the hardness (durability) and enhances oleophobicity / hydrophilicity (switching parameter) of the coatings. The latter is akin to how the roughness of plant leaves can give rise to either hydrophobicity or hydrophilicity depending upon surface functional groups [53,54]. The constituent cationic polymer poly(diallyldimethylammonium) imparts antibacterial properties. Although polymeric quaternary ammonium–surfactant complexes have previously been utilised for their antimicrobial properties, they have not been developed for oil–water separation to provide multi-functional surfaces [55,56]. This concept is important in relation to real-world scenarios, where the simultaneous oil–water separation and killing of bacteria during filtration is highly desirable for safe human water consumption and pollution clean-up.

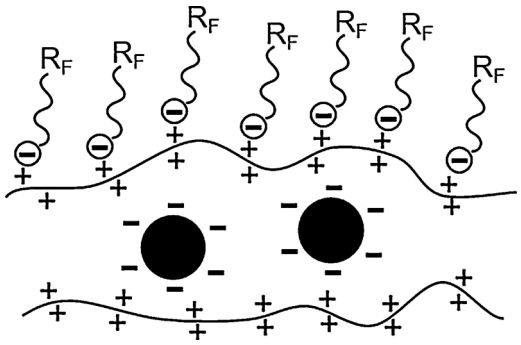

Scheme 1. Cationic poly(diallyldimethylammonium)–anionic fluorosurfactant complex containing negative surface charged nanoparticles.

2. Experimental

2.1. Polymer–particle–fluorosurfactant complex coatings

Aqueous poly(diallyldimethylammonium chloride) (PDDA; Sigma-Aldrich Ltd., 20 wt % in H_2O) was diluted in high-purity water (ISO 3696 grade 2) at a concentration of 2% w/v and the solution allowed to shake for 2 h. If particles were to be incorporated into the coating, then these were ultrasonically dispersed for 1 h in the poly(diallyldimethylammonium chloride) solution at various loadings (loadings are percentage weights by volume (% w/v) of the particle dispersed in the polymer solution). The range of particles investigated are detailed in Table 1.

Anionic phosphate fluorosurfactant (Capstone FS-63, DuPont Ltd.) or amphoteric betaine fluorosurfactant (Capstone FS-50, DuPont Ltd.)

Table 1
Details of the particles used.

Particle	Surface Charge	Average Particle Size	Supplier
SiO_2	Negative	7 nm	Degussa Aerosil® 300
SiO_2	Negative	100 μm	Crosfield Catalysts
SiO_2, methacryloyl functionalised	Negative	12 nm (100–200 nm average aggregate size)	Degussa Aerosil® R711
SiO_2, hexadecylsilane functionalised	Negative	12 nm	Degussa Aerosil® R816
Graphene	Negative	< 2 μm	Strem Chemicals
Al_2O_3	Positive	13 nm	Degussa Aluminiumoxid C
ZnO	Positive	< 100 nm	Sigma-Aldrich Ltd.

were further diluted in high-purity water at a concentration of 5% v/v. The fluorosurfactant solution was added dropwise in a 1:4 vol. ratio to the prepared polymer–particle solution whilst stirring leading to the formation of a polymer–particle–fluorosurfactant complex. The precipitated solid complex was collected from the liquid phase and rinsed with high-purity water followed by drying on a hotplate. The obtained dry solid was dissolved at a concentration of 1% w/v in ethanol (+99.8 wt %, Fisher Scientific UK Ltd.) to provide the coating solution. Glass microscope slides (Academy Science Ltd.) and silicon wafers (Silicon Valley Microelectronics Inc.) were used as flat substrates. These were cleaned prior to coating by sonication in a 50%:50% propan-2-ol (> 99.5 wt %, Fisher Scientific UK Ltd.)/cyclohexane (≥99.7%, Sigma-Aldrich Ltd.) mixture, followed by UV/ozone treatment (BioForce Nanosciences Inc., model UV.TC.EU.003), and finally another sonication step in the propan-2-ol/cyclohexane mixture. Coatings were applied either by solvent casting (solution was dispensed onto the substrate and the solvent allowed to evaporate), or by spray coating using a pressurised spray gun (RG-3 L, Anest Iwata Inc.). For the oil–water separation experiments, stainless steel mesh (#50, 0.20 mm wire diameter, 0.31 mm aperture, The Mesh Company Ltd.) was spray coated. The stainless steel mesh substrates were cleaned prior to coating by rinsing with propan-2-ol.

2.2. Sessile drop contact angle analysis

Sessile drop contact angle analysis was carried out on coated glass slide substrates with a video capture system in combination with a motorised syringe (VCA2500XE, AST Products Inc.). 1 μL droplets of ultrahigh-purity water (BS 3978 grade 1) and hexadecane (99%, Sigma-Aldrich Ltd.) were dispensed for water and oil contact angle measurements respectively. Following dispensation of the probe liquid onto the coated substrate, a snapshot of the image was taken and analysed using the VCA-2500 Dynamic/Windows software. The water contact angle (WCA) was measured as soon as the droplet was placed onto the surface and again after a period of 10 s—this was done in order to observe any change in the WCA over a short time period due to the "switching" behaviour of these surfaces (a short time of 10 s was chosen because coatings required for oil–water separation applications need to switch quickly in order to attain high efficiencies). The hexadecane contact angle (HCA) was measured as soon as the droplet was placed onto the surface and it was observed not to vary with time. The reported contact angle measurements were made after rinsing samples with water and drying in air. Switching parameters were determined by calculating the difference between the equilibrium hexadecane and water static contact angles.

2.3. Captive bubble

Captive bubble contact angle analysis was carried out on coated glass slide substrates with the video capture system in combination with a captive bubble attachment dispensing approximately 1 μL air bubbles (VCA captive bubble accessory, AST Products Inc.). Following release of the air bubble onto the coated substrate under water, the droplet was viewed using the VCA-2500 Dynamic/Windows software.

2.4. Scanning electron microscopy

Coated silicon wafer substrates were mounted onto carbon disks supported on aluminium stubs, and then coated with a thin gold layer (5–10 nm, Polaron SEM Coating Unit, Quorum Technologies Ltd.). Surface morphology images were acquired using a scanning electron microscope (model Vega 3LMU, Tescan Orsay Holdings a.s.) operating in secondary electron detection mode, in conjunction with an 8 kV accelerating voltage, and a working distance of 8–11 mm.

2.5. Microindentation

Hardness values were obtained for coated silicon wafer substrates using a microhardness tester (model MVK-H2, Mitutoyo Inc.) fitted with a standard Vickers tip. Five microindentation measurements were made across the surface for each applied force (international standard ASTM E384–11e1) [57].

2.6. Oil–water separation

Oil–water separation experiments were carried out using the coated stainless steel mesh substrates. An agitated mixture of oil (hexadecane, 99%, Sigma-Aldrich Ltd.) and water (high-purity, ISO 3696 grade 2) was poured over the stainless steel mesh. The mesh was either placed horizontally above one beaker or at an incline above two beakers for batch and continuous separations respectively. In order to enhance the visual contrast, Oil Red O (≥75% dye content, Sigma-Aldrich Ltd.) and Procion Blue MX-R (35% dye content, Sigma-Aldrich Ltd.) were added to the oil (red) and water (blue) respectively.

2.7. Antibacterial activity

Gram-negative *Escherichia coli* BW25113 (CGSC 7636; *rrnB3 ΔlacZ4787 hsdR514 Δ(araBAD)567 Δ(rhaBAD)568 rph-1*) and Gram-positive *Staphylococcus aureus* (FDA209P, an MSSA strain; ATCC 6538P) bacterial cultures were prepared using autoclaved (Autoclave Vario 1528, Dixons Ltd.) Luria-Bertani broth (L3022, Sigma-Aldrich Ltd.) media (2% w/v in Milli-Q water). A 5 mL bacterial culture was grown from a single colony for 16 h at 37 °C and 50 μL used to inoculate a sterile polystyrene cuvette (67.742, Sarstedt AG) containing Luria-Bertani broth (1 mL). The cuvette was covered with Parafilm (Cole-Parmer Ltd.) and then placed inside a bacterial incubator shaker (Stuart Orbital Incubator S1500, Cole-Parmer Ltd.) set at 37 °C and 120 rpm. An optical density $OD_{650nm} = 0.4$ was verified using a spectrophotometer (BOECO S-30, Boeckel GmbH) to obtain bacteria at the mid-log phase of growth.

Pieces of non-woven polypropylene sheet (0.11 mm thickness, 22.7 ± 1.1 μm fibre diameter, Spunbound, 70 g m^{-2}, Avoca Technical Ltd., UK) were spray coated with either poly(diallyldimethylammonium)–anionic fluorosurfactant complex or poly(diallyldimethylammonium)–3% w/v silica (7 nm)–anionic fluorosurfactant complex solutions, and the carrier solvent allowed to evaporate. Uncoated control samples were washed in absolute ethanol for 15 min and then dried under vacuum in order to make sure they were sterile and clean. At least 4 different batches of each type of coated sample, as well as the control uncoated non-woven polypropylene sheet, were tested for antimicrobial activity.

Sterile microtubes (1.5 mL, Sarstedt AG) were loaded with the uncoated, polymer–fluorosurfactant or polymer–nanoparticle–-fluorosurfactant coated non-woven polypropylene sheet. Next, 100 μL of the prepared bacteria solution was placed onto each sheet (so that the microorganisms could interact with the surface), and left to incubate (Bacterial Incubator 250, LMS Ltd.) at 30 °C for 16 h. Next, autoclaved Luria-Bertani broth media (900 μL) was pipetted into each microtube and vortexed (Vortex-Genie 2, Scientific Industries Inc.) in order to recover the bacteria as a 10-fold dilution (10^{-1}). Further ten-fold serial dilutions were performed to give 10^{-2}, 10^{-3}, 10^{-4}, 10^{-5} and 10^{-6} samples. Colony-forming unit (CFU) plate counting was performed by placing 10 μL drops from each sample onto autoclaved Luria-Bertani solid agar plates (EZMix™ powder, dust free, fast dissolving fermentation medium, L7533, Sigma-Aldrich Ltd.) and incubated (Bacterial Incubator 250, LMS Ltd.) at 30 °C for 16 h. The number of colonies visible at each dilution were then counted.

3. Results and discussion

3.1. Sessile drop contact angle

Oleophobic–hydrophilic surfaces were prepared using either anionic or amphoteric fluorosurfactants in combination with poly(diallyldimethylammonium chloride), Scheme 1. The oleophobicity of polymer–fluorosurfactant complex surfaces can be attributed to the fluorinated surfactant tails being orientated towards the air–solid interface exposing the low surface energy terminal CF_3 groups [43]. Consequently, the hydrophilic ionic surfactant head groups and the complexed polymer counterionic groups are buried within the subsurface region. When droplet water molecules come into contact with these polymer–fluorosurfactant surfaces, they are able to diffuse towards these underlying hydrophilic groups via one of two mechanisms: either the water molecules wick down towards the hydrophilic subsurface region due to defects at the air–solid interface [44], or the hydrophilic subsurface is exposed to the water molecules as a consequence of water-induced molecular rearrangement of the fluorinated chains [47]. Both mechanisms can account for the time-dependent hydrophilicity of the polymer–fluorosurfactant complex surfaces (it either takes time for the water molecules to penetrate through the defects, or it takes time for the fluorinated chains to orientate during the water-induced molecular rearrangement). The oleophobic behaviour can also be accounted for on the basis of either mechanism. In the case of the defect mechanism, the much larger oil molecules are unable to penetrate any film defects, and so only come into contact with the low surface energy fluorinated tails. Alternatively, if the mechanism involves a water-induced molecular rearrangement, then the oleophobicity occurs as a result of the fluorinated chains remaining exposed at the air–solid interface when in contact with oil. Hence, the polymer–fluorosurfactant complex surfaces display the observed switching oleophobic–hydrophilic properties (the difference between the static water and oil contact angles). Previously reported polymer–fluorosurfactant complex surfaces have tended to exhibit relatively small switching parameters [34,35,37,43,47,48] (usually as a result of poor oleophobicity) or display long switching times [40,41] (taking several minutes for the water droplets to fully wet the surface). Furthermore, the current single-step application methodology is far more straightforward compared to earlier lengthy layer-by-layer approaches involving multiple steps.[39]

Nanoparticle incorporation into these coatings led to an enhancement in the switching parameter (the difference between the equilibrium oil and water static contact angles) by either decreasing the water contact angle (WCA) or by increasing the hexadecane contact angle (HCA)—optimally a combination of both, Fig. 1. This improvement in surface oleophobicity and hydrophilicity relative to the nanoparticle-free control samples can be attributed to the impact of surface roughening upon Wenzel [58] and Wenzel/Cassie–Baxter [59] states of wetting respectively. Eventually, a critical nanoparticle loading value is reached beyond which the switching behaviour starts to deteriorate. Prior to a drop in performance, the poly(diallyldimethylammonium)–anionic fluorosurfactant complex system was found to accommodate higher loadings of 7 nm silica nanoparticles (3% w/v) compared to the poly(diallyldimethylammonium)–amphoteric fluorosurfactant complex system (1.5% w/v), and therefore the former was chosen for further investigation. At these optimum nanoparticle loadings, the surface became completely wetting towards water within 10 s, Supplementary Material Table S 1 and Table S 2. Such hydrophilicity is suitable for anti-fogging applications [42]. Similar trends were observed for both spray coating and solvent casting methods of application. Such incorporation of nanoparticles into coating surfaces mimic nanoscale roughness widely found on plant surfaces for the enhancement of liquid wettability [60] / repellency [61].

A range of other unfunctionalised and functionalised negatively charged nano- and micron-size particles were also found to enhance the switching parameter (this can be attributed to their electrostatic ability to complex to the positively charged polymer backbone), Fig. 2. On the other hand, positively charged alumina and zinc oxide nanoparticles performed less well. In the case of alumina nanoparticles, their inclusion at a loading of 3% w/v gave rise to a detrimental effect on the switching parameter stemming from a large rise in the water contact angle. Alkyl functionalised silica nanoparticles showed greater oleophobicity at low loadings (1% w/v) compared to unfunctionalised silica nanoparticles—this is probably due to the surface alkyl group oleophobicity. At higher loadings (3% w/v), the alkyl functionalisation of nanoparticles appeared not to provide any significant advantage, Fig. 2. Given that the poly(diallyldimethylammonium)–anionic fluorosurfactant complex system with 3% w/v loading of 7 nm silica nanoparticles displayed the largest switching parameter, this was selected for further investigation.

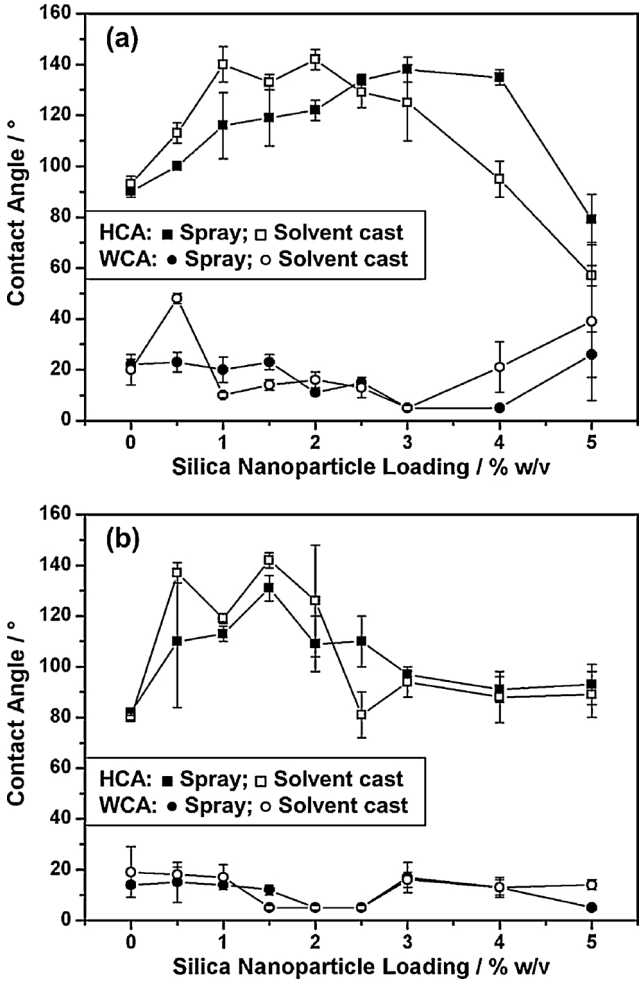

Fig. 1. Water contact angle (WCA after 10 s) and hexadecane contact angle (HCA) for coated flat glass substrates as a function of 7 nm silica nanoparticle loading concentration in poly(diallyldimethylammonium)–silica precursor solution mixed with: (a) anionic fluorosurfactant; and (b) amphoteric fluorosurfactant.

3.2. Captive bubble contact angle

For the superhydrophilic poly(diallyldimethylammonium)–3% w/v silica (7 nm)–anionic fluorosurfactant and poly(diallyldimethylammonium)–1.5% w/v silica (7 nm)–amphoteric fluorosurfactant complex coated substrates, it was found that the air bubble did not release from the needle upon contact with the sample surfaces (superhydrophilicity [62]). Increasing the size of the air bubble until it eventually released from the needle led to the bubble simply rising towards the sample

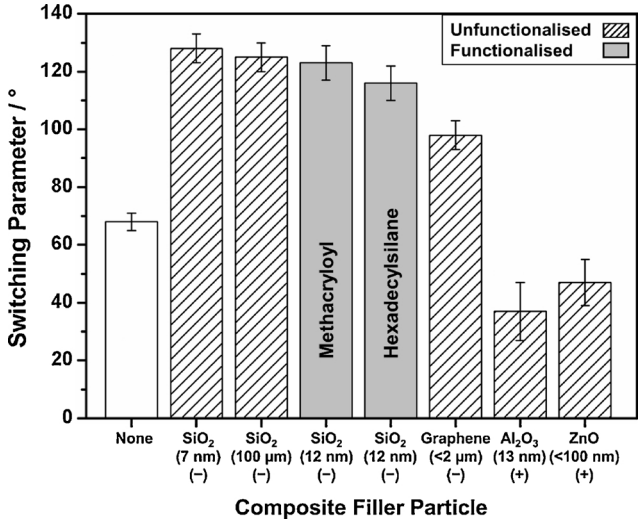

Fig. 2. Oleophobic–hydrophilic switching parameters for various spray coated poly(diallyldimethylammonium)–particle–anionic fluorosurfactant complex coatings at 3% w/v particle loading in poly(diallyldimethylammonium)–particle precursor solution. Switching parameters are calculated from the difference between the hexadecane and water static contact angles (after 10 s). Nanoparticle surface charge is indicated within brackets as (−) or (+).

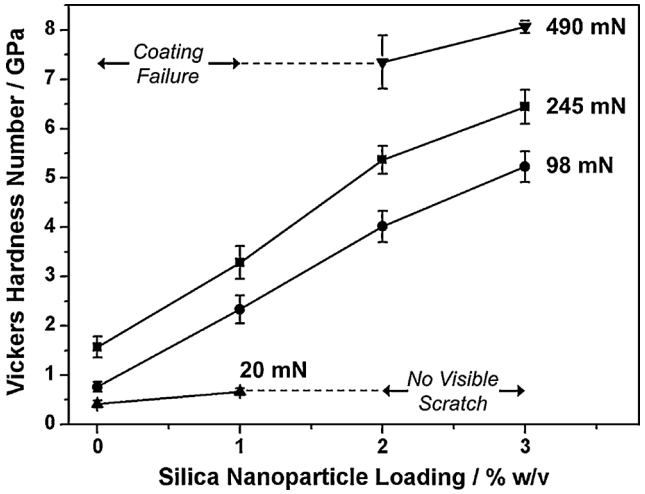

Fig. 4. Vickers hardness number measured for various applied microindentation forces as a function of 7 nm silica nanoparticle loading concentration for poly(diallyldimethylammonium)–silica–anionic fluorosurfactant spray coated onto silicon wafer substrates.

followed by running along the coating surface and off the edge, Supplementary Material Video S1. Hence, the captive bubble contact angle value of 180° correlates to the calculated WCA of 0° (at 10 s) from the sessile drop technique [63]. This surface hydrophilicity (low water contact angle) can be attributed to a water layer being present on the surface—the water layer effectively repels the air bubble preventing it from adhering to the coating surface [64].

The difference observed between the sessile drop and the captive bubble methods for measurements made at $t = 0$ s is because the timescale to "switch" is about 10 s for the former, whereas the prior immersion of sample into water for the latter has already caused the surface rearrangement ("switch")—thereby effectively making the captive bubble WCA unchanged between $t = 0$ s and $t = 10$ s.

3.3. Scanning electron microscopy

Scanning electron microscopy (SEM) showed that in the absence of silica nanoparticles, the coatings are relatively smooth with any minor roughness features attributable to the spray coating process, Fig. 3. The incorporation of nanoparticles enhances the coating surface roughness for both the poly(diallyldimethylammonium)–anionic fluorosurfactant and poly(diallyldimethylammonium)–amphoteric fluorosurfactant systems. The scale of the surface roughness features is approximately

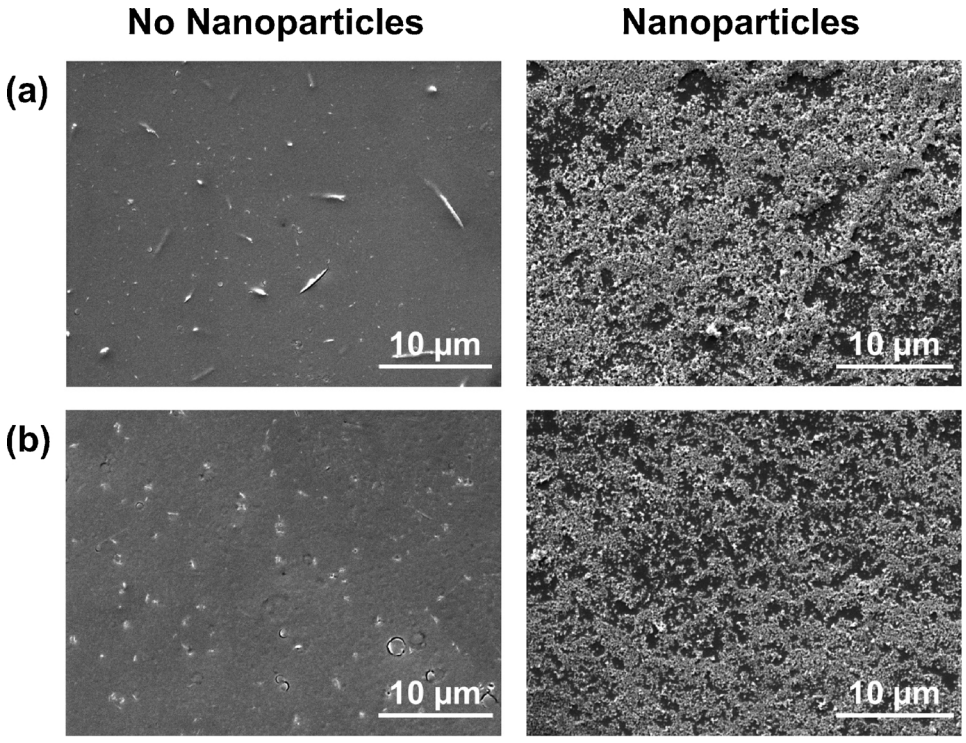

Fig. 3. SEM images of spray coatings with and without nanoparticles: (a) poly(diallyldimethylammonium)–anionic fluorosurfactant; and (b) poly(diallyldimethylammonium)–amphoteric fluorosurfactant. The silica (7 nm) nanoparticle loadings correspond to the best switching parameters (3% w/v and 1.5% w/v for (a) and (b) respectively). Higher resolution images are shown in Supplementary Material Figure S1.

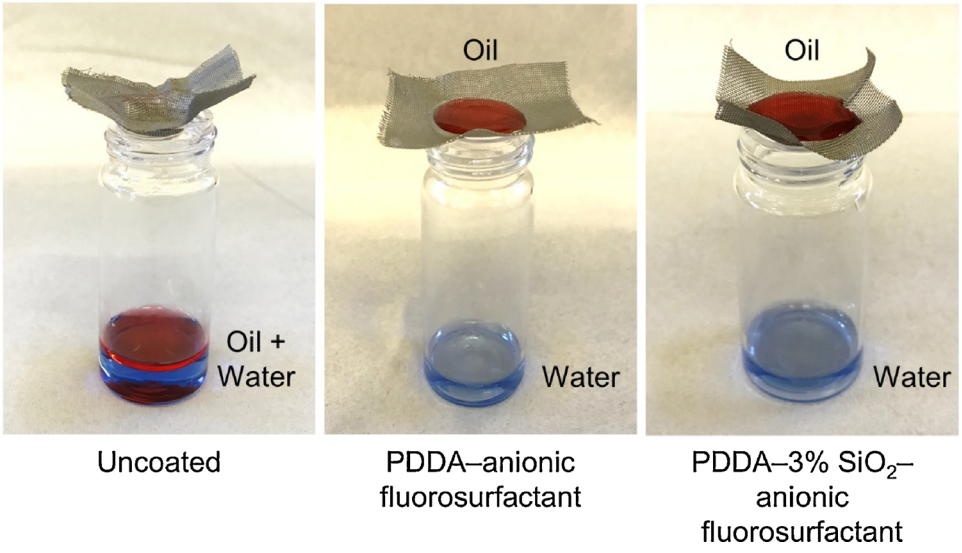

Fig. 5. Oil (hexadecane)–water separation performance of uncoated mesh, poly(diallyldimethylammonium)–anionic fluorosurfactant complex spray coated mesh, and poly(diallyldimethylammonium)–3% w/v silica (7 nm)–anionic fluorosurfactant spray coated mesh. See also Supplementary Material Figure S2 and Video S2. Poly(diallyldimethylammonium) is abbreviated as PDDA.

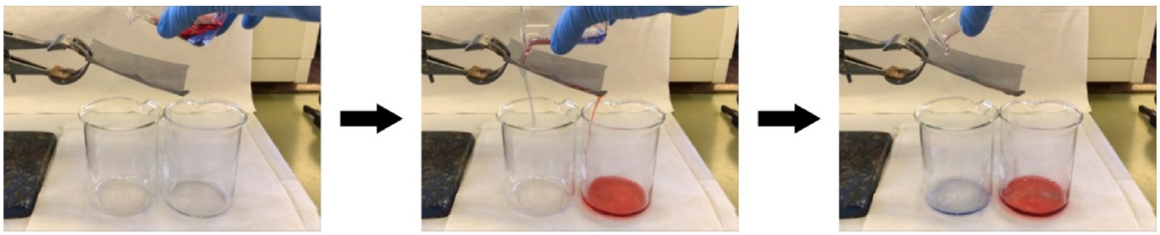

Fig. 6. Separation of an oil (hexadecane)–water mixture using a poly(diallyldimethylammonium)–3% w/v silica (7 nm)–anionic fluorosurfactant spray coated mesh. Oil is dyed red and water is dyed blue. (For interpretation of the references to colour in this figure legend, the reader is referred to the web version of this article.).

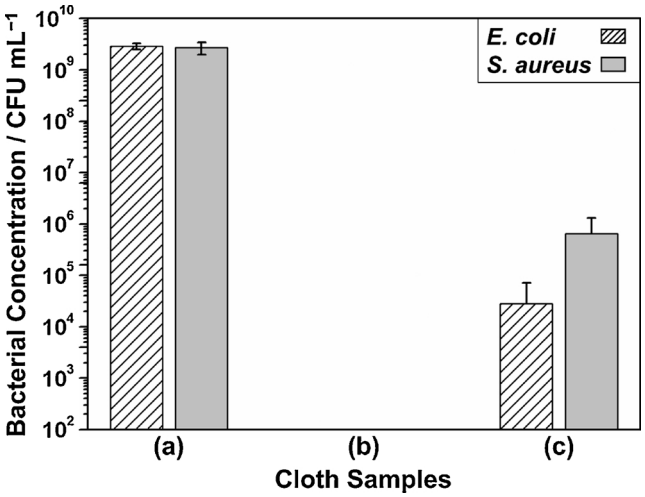

Fig. 7. Antibacterial activity against *E. coli* (Gram-negative) and *S. aureus* (Gram-positive) bacteria: (a) untreated non-woven polypropylene sheet control; (b) poly(diallyldimethylammonium)–anionic fluorosurfactant complex spray coated non-woven polypropylene sheet; (c) poly(diallyldimethylammonium)–3% w/v silica (7 nm)–anionic fluorosurfactant spray coated non-woven polypropylene sheet. Reported values are averaged over at least 4 different values with standard deviation error.

100–200 nm in size which is consistent with there being encapsulation of the nanoparticles within the polymer–fluorosurfactant complex host matrix (rather than due to discrete individual 7 nm silica nanoparticles).

3.4. Hardness

Microindentation measurements showed that for a given indentation force, the hardness improved with rising silica nanoparticle loading, Fig. 4. In the absence of or at low loadings of silica nanoparticles (1% w/v silica), a large indentation force of 490 mN was sufficient to pierce through the coatings causing the underlying silicon substrate to crack (i.e. a hardness value could not be measured at this high force). At low indentation forces (20 mN), the coatings with 2% w/v and 3% w/v nanoparticle loadings displayed no visible indent (i.e. scratch-resistant). Therefore, a force of 98 mN or 245 mN was employed in order to follow the effect of varying silica loading—both forces showed that the hardness increases with rising silica loading, Fig. 4.

3.5. Oil–water separation

Poly(diallyldimethylammonium)–anionic fluorosurfactant complex and poly(diallyldimethylammonium)–3% w/v silica (7 nm)–anionic fluorosurfactant coated horizontal meshes displayed oil–water separation behaviour, Fig. 5. High-purity water passed through both uncoated and coated meshes, whilst oil (hexadecane) did not pass through the coated mesh—thereby demonstrating that the coated mesh can separate oil from water with 100% efficiency.

By inclining the coated meshes above two beakers, oil–water mixtures could be separated into the respective beakers, Fig. 6 and Supplementary Material Video S3. The small amount of water (less than 5% vol.) which passes into the oil beaker is due to some of the water being dragged along by the oil across the mesh as it passes across it, and could be easily removed by repeating the procedure. The oil–water separation is highly reproducible with over 50 coatings having been tested. Similar performance was measured for vegetable cooking oil, Supplementary Material Video S 4.

3.6. Antibacterial activity

E. coli bacteria often found in drinking water supplies [65] and *S. aureus* bacteria present in seawater [66] are both harmful to human health. The control untreated non-woven polypropylene sheet displayed *E. coli* and *S. aureus* bacterial counts of $2.88 \pm 0.39 \times 10^9$ CFU mL^{-1} at 10^{-6} dilution ($n = 6$, standard deviation error) and $2.70 \pm 0.73 \times 10^9$ CFU mL^{-1} at 10^{-6} dilution (n = 4, standard deviation error) respectively, Fig. 7. Both poly(diallyldimethylammonium)–anionic fluorosurfactant and poly(diallyldimethylammonium)–3% w/v silica (7 nm)–anionic fluorosurfactant complex coated non-woven polypropylene sheets showed high antibacterial activity against the *E. coli* and *S. aureus* bacteria tested. The former reduced the number of both *E. coli* and *S. aureus* bacteria to zero at 10^{-1} dilution, whilst the latter exceeded +99.99% killing ($2.83 \pm 4.34 \times 10^4$ CFU mL^{-1}) of *E. coli* bacteria at 10^{-2} dilution ($n = 6$, standard deviation error) and +99.97% killing ($6.50 \pm 6.65 \times 10^5$ CFU mL^{-1}) of *S. aureus* bacteria at 10^{-3} dilution (n = 4, standard deviation error), Fig. 7.

Such utilisation of cationic poly(diallyldimethylammonium) polymers for fluorosurfactant complex formation incorporates the added benefit of antibacterial poly(diallyldimethylammonium) quaternary ammonium centres [67,68]. These antimicrobial properties arise due to the interactions of the positively charged ammonium group with the negatively charged head groups of phospholipids in bacterial membranes which cause disruption of the membrane leading to cell leakage and eventually cell death [69–71]. The measured +99.99% (*E. coli*) and +99.97% (*S. aureus*) bacterial kill rate for poly(diallyldimethylammonium)–3% w/v silica (7 nm)–anionic fluorosurfactant complex coated non-woven polypropylene sheets can be attributed to surface roughness lowering available anchoring points for bacteria attachment (reduction in available area of contact with the bacteria's outer surface [72]). The small difference in bacteria kill rates between *E. coli* and *S. aureus* for poly(diallyldimethylammonium)–3% w/v silica (7 nm)–anionic fluorosurfactant complex coated non-woven polypropylene sheets may be due to differences in the outer surface structures of the two species [73].

4. Conclusions

Multifunctional fast-switching oleophobic–hydrophilic coatings have been prepared using polymer–nanoparticle–fluorosurfactant complexes. These can be deposited in a single step by spraying or solvent-casting. Electrostatic attraction of negatively charged nanoparticles (silicas and graphene) within cationic poly(diallyldimethylammonium)–anionic fluorosurfactant complex films introduces surface roughening which enhances hydrophilicity and oleophobicity as a consequence of Wenzel and Wenzel/Cassie–Baxter wetting states respectively. These surfaces provide high-efficiency continuous oil–-water separation. Nanoparticle incorporation also improves coating hardness (durability). The cationic polymer quaternary ammonium centres present within these polymer–nanoparticle–fluorosurfactant complex systems impart antibacterial surface properties (including against water-borne *E. coli* (Gram-negative) and *S. aureus* (Gram-positive) bacteria). Other applications include antibacterial–antifogging surfaces.

Conflicts of interest

There are no conflicts of interest to declare.

Funding

This work was supported by Engineering and Physical Sciences Research Council (EPSRC—grant reference EP/J005401/1 and studentship reference EP/M507854/1), and British Council (Katip Çelebi – Newton Fund grant reference 333595). S. N. B.-P. was funded by Consejo Nacional de Ciencia y Tecnología, Mexico (CONACyT) scholarship reference 409090.

Author contributions

J. P. S. B. devised the concept. A. W. R. carried out sample preparation and liquid repellency studies. H. J. C., S. N. B.-P., and G. J. S. performed antibacterial testing. The manuscript was jointly drafted by J. P. S. B. and A. W. R. All authors gave final approval for publication.

Data access

Data created during this research can be accessed at: https://collections.durham.ac.uk.

Acknowledgements

We thank T. Davey of the Electron Microscopy Research Services at Newcastle University for the SEM imaging and J. J. Wu of the School of Engineering and Computing Sciences at Durham University for providing access to microindentation measurements.

Appendix A. Supplementary data

Supplementary material related to this article can be found, in the online version, at doi:https://doi.org/10.1016/j.colsurfa.2018.10.030.

References

[1] P.F. Kingston, Long-term environmental impact of oil spills, Spill Sci. Technol. Bull. 7 (2002) 53–61.
[2] L.P. Gossen, L.M. Velichkina, Environmental problems of the oil-and-gas industry, Pet. Chem. 46 (2006) 67–72.
[3] I.B. Ivshina, M.S. Kuyukina, A.V. Krivoruchko, A.A. Elkin, S.O. Makarov, C.J. Cunningham, T.A. Peshkur, R.M. Atlas, J.C. Philp, Oil spill problems and sustainable response strategies through new technologies, Environ. Sci.: Process. Impacts 17 (2015) 1201–1219.
[4] S.B. Joye, Deepwater horizon, 5 years on, Science 349 (2015) 592–593.
[5] B. Dubansky, A. Whitehead, J.T. Miller, C.D. Rice, F. Galvez, Multitissue molecular, genomic, and developmental effects of the deepwater horizon oil spill on resident gulf killifish (*Fundulus grandis*), Environ. Sci. Technol. 47 (2013) 5074–5082.
[6] C.H. Peterson, S.D. Rice, J.W. Short, D. Esler, J.L. Bodkin, B.E. Ballachey, D.B. Irons, Long-term ecosystem response to the Exxon Valdez oil spill, Science 302 (2003) 2082–2086.
[7] H.–M. Choi, R.M. Cloud, Natural sorbents in oil spill cleanup, Environ. Sci. Technol. 26 (1992) 772–776.
[8] Ch. Teas, S. Kalligeros, F. Zanikos, S. Stournas, E. Lois, G. Anastopoulos, Investigation of the effectiveness of absorbent materials in oil spill clean up, Desalination 140 (2001) 259–264.
[9] M.O. Adebajo, R.L. Frost, J.T. Kloprogge, O. Carmody, S. Kokot, Porous materials for oil spill cleanup: a review of synthesis and absorbing properties, J. Porous Mater. 10 (2003) 159–170.
[10] A. Bayat, S.F. Aghamiri, A. Moheb, G.R. Vakili-Nezhaad, Oil spill cleanup from sea water by sorbent materials, Chem. Eng. Technol. 28 (2005) 1525–1528.
[11] Y. Yang, Z. Liu, J. Huang, C. Wang, Multifunctional, robust sponges by a simple adsorption–combustion method, J. Mater. Chem. A 3 (2015) 5875–5881.
[12] D. Ceylan, S. Dogu, B. Karacik, S.D. Yakan, O.S. Okay, O. Okay, Evaluation of butyl rubber as sorbent material for the removal of oil and polycyclic aromatic hydrocarbons from seawater, Environ. Sci. Technol. 43 (2009) 3846–3852.
[13] X. Zhou, Z. Zhang, X. Xu, X. Men, X. Zhu, Facile fabrication of superhydrophobic sponge with selective absorption and collection of oil from water, Ind. Eng. Chem. Res. 52 (2013) 9411–9416.
[14] J.A. Howarter, J.P. Youngblood, Amphiphile grafted membranes for the separation of oil-in-water dispersions, J. Colloid Interface Sci. 329 (2009) 127–132.
[15] A.K. Kota, G. Kwon, W. Choi, J.M. Mabry, A. Tuteja, Hygro-responsive membranes for effective oil–water separation, Nat. Commun. 3 (2012) 1025.
[16] G. Kwon, A.K. Kota, Y. Li, A. Sohani, J.M. Mabry, A. Tuteja, On-demand separation of oil–water mixtures, Adv. Mater. 24 (2012) 3666–3671.
[17] S. Pan, R. Guo, W. Xu, Durable superoleophobic fabric surfaces with counter-intuitive superwettability for polar solvents, AIChE J. 60 (2014) 2752–2756.
[18] Z. Xu, Y. Zhao, H. Wang, X. Wang, T. Lin, A superamphiphobic coating with an ammonia-triggered transition to superhydrophilic and superoleophobic for oil–-water separation, Angew. Chem. Int. Ed. 54 (2015) 4527–4530.
[19] G. Kwon, E. Post, A. Tuteja, Membranes with selective wettability for the separation of oil–water mixtures, MRS Commun. 5 (2015) 475–494.
[20] T. Shen, S. Li, Z. Wang, L. Wang, Rare Bi-wetting TiO_2-F/SiO_2/F-PEG fabric coating for self-cleaning and oil/water separation, RSC Adv. 6 (2016) 115196–115203.

[21] C. Crick, J.A. Gibbins, I.P. Parkin, Superhydrophobic polymer-coated copper-mesh; membranes for highly efficient oil–water separation, J. Mater. Chem. A 1 (2013) 5943–5948.
[22] L. Feng, Z. Zhang, Z. Mai, Y. Ma, B. Liu, L. Jiang, D. Zhu, A super-hydrophobic and super-oleophilic coating mesh film for the separation of oil and water, Angew. Chem. Int. Ed. 43 (2004) 2012–2014.
[23] C. Wang, T. Yao, J. Wu, C. Ma, Z. Fan, Z. Wang, Y. Cheng, Q. Lin, B. Yang, Facile approach in fabricating superhydrophobic and superoleophilic surface for water and oil mixture separation, ACS Appl. Mater. Interfaces 1 (2009) 2613–2617.
[24] D.D. Nguyen, N.H. Tai, S.B. Lee, W.S. Kuo, Superhydrophobic and superoleophilic properties of graphene-based sponges fabricated using a facile dip coating method, Energy Environ. Sci. 5 (2012) 7908–7912.
[25] C.H. Lee, N. Johnson, J. Drelich, Y.K. Yap, The performance of superhydrophobic and superoleophilic carbon nanotube meshes in water–oil filtration, Carbon 49 (2011) 669–676.
[26] J.A. Howarter, J.P. Youngblood, Self-cleaning and anti-fog surfaces via stimuli-responsive polymer brushes, Adv. Mater. 19 (2007) 3838–3843.
[27] Z. Xue, S. Wang, L. Lin, L. Chen, M. Liu, L. Feng, L. Jiang, A novel superhydrophilic and underwater superoleophobic hydrogel-coated mesh for oil/water separation, Adv. Mater. 23 (2011) 4270–4273.
[28] Y. Zhu, F. Zhang, D. Wang, X.F. Pei, W. Zhang, J. Jin, A novel zwitterionic polyelectrolyte grafted PVDF membrane for thoroughly separating oil from water with ultrahigh efficiency, J. Mater. Chem. A 1 (2013) 5758–5765.
[29] X. Gao, L.–P. Xu, Z. Xue, L. Feng, J. Peng, Y. Wen, S. Wang, X. Zhang, Dual-scaled porous nitrocellulose membranes with underwater superoleophobicity for highly efficient oil/water separation, Adv. Mater. 26 (2014) 1771–1775.
[30] M.A. Gondal, M.S. Sadullah, M.A. Dastageer, G.H. McKinley, D. Panchanathan, K.K. Varanasi, Study of factors governing oil–water separation process using TiO_2 films prepared by spray deposition of nanoparticle dispersions, ACS Appl. Mater. Interfaces 6 (2014) 13422–13429.
[31] J.A. Howarter, J.P. Youngblood, Self-cleaning and next generation anti-fog surfaces and coatings, Macromol. Rapid Commun. 29 (2008) 455–466.
[32] J.A. Howarter, K.L. Genson, J.P. Youngblood, Wetting behavior of oleophobic polymer coatings synthesized from fluorosurfactant-macromers, ACS Appl. Mater. Interfaces 3 (2011) 2022–2030.
[33] Y. Wang, Q. Dong, Y. Wang, H. Wang, G. Li, R. Bai, Investigation on RAFT polymerization of a Y-shaped amphiphilic fluorinated monomer and anti-fog and oil-repellent properties of the polymers, Macromol. Rapid Commun. 31 (2010) 1816–1821.
[34] M. Antonietti, S. Henke, A. Thünemann, Highly ordered materials with ultra-low surface energies: polyelectrolyte–surfactant complexes with fluorinated surfactants, Adv. Mater. 8 (1996) 41–45.
[35] S. Turri, R. Valsecchi, M. Viganò, M. Levi, Hydrophilic–oleophobic behaviour in thin films from fluoromodified nanoclays and polystyrene, Polym. Bull. 63 (2009) 235–243.
[36] E.D. Goddard, Polymer–surfactant interaction part II. Polymer and surfactant of opposite charge, Colloids Surf. 19 (1986) 301–329.
[37] A.F. Thünemann, K.H. Lochhaas, Surface and solid-state properties of a fluorinated polyelectrolyte–surfactant complex, Langmuir 15 (1999) 4867–4874.
[38] H. Tang, Y. Fu, C. Yang, D. Zhu, J. Yang, A UV-driven superhydrophilic/superoleophobic polyelectrolyte multilayer film on fabric and its application in oil/water separation, RSC Adv. 6 (2016) 91301–91307.
[39] P.S. Brown, B. Bhushan, Mechanically durable, superoleophobic coatings prepared by layer-by-layer technique for anti-smudge and oil–water separation, Sci. Rep. 5 (2015) 8701.
[40] J. Yang, Z. Zhang, X. Xu, X. Zhu, X. Men, X. Zhou, Superhydrophilic–superoleophobic coatings, J. Mater. Chem. 22 (2012) 2834–2837.
[41] J. Yang, L. Yin, H. Tang, H. Song, X. Gao, K. Liang, C. Li, Polyelectrolyte–fluorosurfactant–complex–based meshes with superhydrophilicity and superoleophobicity for oil/water separation, Chem. Eng. J. 268 (2015) 245–250.
[42] P.S. Brown, O.D.L.A. Atkinson, J.P.S. Badyal, Ultrafast oleophobic–hydrophilic switching surfaces for antifogging, self-cleaning, and oil–water separation, ACS Appl. Mater. Interfaces 6 (2014) 7504–7511.
[43] A.F. Thünemann, A. Lieske, B.–R. Paulke, Low surface energy coatings from waterborne nano-dispersions of polymer complexes, Adv. Mater. 11 (1999) 321–324.
[44] L. Li, Y. Wang, C. Gallaschun, T. Risch, J. Sun, Why can a nanometer-thick polymer coated surface be more wettable to water than to oil? J. Mater. Chem. 22 (2012) 16719–16722.
[45] Y. Wang, J. Knapp, A. Legere, J. Raney, L. Li, Effect of end-groups on simultaneous oleophobicity/hydrophilicity and anti-fogging performance of nanometer-thick perfluoropolyethers (PFPEs), RSC Adv. 5 (2015) 30570–30576.
[46] Y. Wang, M. Dugan, B. Urbaniak, L. Li, Fabricating nanometer-thick simultaneously oleophobic/hydrophilic polymer coatings via a photochemical approach, Langmuir 32 (2016) 6723–6729.
[47] H. Yoon, S.H. Na, J.Y. Choi, S.S. Latthe, M.T. Swihart, S.S. Al-Deyab, S.S. Yoon, Gravity-driven hybrid membrane for oleophobic–superhydrophilic oil–water separation and water purification by graphene, Langmuir 30 (2014) 11761–11769.
[48] A.F. Thünemann, U. Schnöller, O. Nuyken, B. Voit, Self-assembled complexes of diazosulfonate polymers with low surface energies, Macromolecules 32 (1999) 7414–7421.
[49] R.A. Lampitt, J.M. Crowther, J.P.S. Badyal, Switching liquid repellent surfaces, J. Phys. Chem. B 104 (2000) 10329–10331.
[50] S.J. Hutton, J.M. Crowther, J.P.S. Badyal, Complexation of fluorosurfactants to functionalized solid surfaces: smart behavior, Chem. Mater. 12 (2000) 2282–2286.
[51] R. Molina, M. Gómez, C.–W. Kan, E. Bertran, Hydrophilic–oleophobic coatings on cellulosic materials by plasma assisted polymerization in liquid phase and fluorosurfactant complexation, Cellulose 21 (2014) 729–739.
[52] P.S. Brown, B. Bhushan, Bioinspired, roughness-induced, water and oil super-philic and super-phobic coatings prepared by adaptable layer-by-layer technique, Sci. Rep. 5 (2015) 14030.
[53] K. Koch, W. Barthlott, Superhydrophobic and superhydrophilic plant surfaces: an inspiration for biomimetic materials, Phil. Trans. R. Soc. A 367 (2009) 1487–1509.
[54] G. Wen, Z. Guo, W. Liu, Biomimetic polymeric superhydrophobic surfaces and nanostructures: from fabrication to applications, Nanoscale 9 (2017) 3338–3366.
[55] K. Ushimaru, Y. Hamano, H. Katano, Antimicrobial activity of ε-poly-L-lysine after forming a water-insoluble complex with an anionic surfactant, Biomacromolecules 18 (2017) 1387–1392.
[56] M. Ashiuchi, Y. Hakumai, S. Nakayama, H. Higashiuchi, K. Shimada, Engineering antimicrobial coating of archael poly-γ-glutamate-based materials using non-covalent crosslinkages, Sci. Rep. 8 (2018) 4645.
[57] ASTM Standard E384–11e1, Standard Test Method for Knoop and Vickers Hardness of Materials, ASTM International, West Conshohocken, PA, 2011, https://doi.org/10.1520/E0384-11E01 www.astm.org.
[58] R.N. Wenzel, Resistance of solid surfaces to wetting by water, Ind. Eng. Chem. 28 (1936) 988–994.
[59] A.B.D. Cassie, S. Baxter, Wettability of porous surfaces, Trans. Faraday Soc. 40 (1944) 546–551.
[60] H.F. Bohn, W. Federle, Insect aquaplaning: *Nepenthes* Pitcher plants capture prey with the peristome, a fully wettable water-lubricated anisotropic surface, Proc. Natl. Acad. Sci. U. S. A. 101 (2004) 14138–14143.
[61] W. Barthlott, C. Neinhuis, Purity of the sacred lotus, or escape from contamination in biological surfaces, Planta 202 (1997) 1–8.
[62] C. Dorrer, J. Rühe, Superaerophobicity: repellence of air bubbles from submerged, surface-engineered silicon substrates, Langmuir 28 (2012) 14968–14973.
[63] F.J. Montes Ruiz-Cabello, M.A. Rodriguez-Valverde, A. Marmur, M.A. Cabrerizo-Vilchez, Comparison of sessile drop and captive bubble methods on rough homogeneous surfaces: a numerical study, Langmuir 27 (2011) 9638–9643.
[64] M. Morra, E. Occhiello, F. Garbassi, The wetting behavior of grafted hydrophilic acrylic monomers, Colloid Polym. Sci. 271 (1993) 696–704.
[65] S.C. Edberg, E.W. Rice, R.J. Karlin, M.J. Allen, *Escherichia coli*: the best biological drinking water indicator for public health protection, J. Appl. Microbiol. 88 (2000) 106S–116S.
[66] L.R.W. Plano, A.C. Garza, T. Shibata, S.M. Elmir, J. Kish, C.D. Sinigalliano, M.L. Gidley, G. Miller, K. Withum, L.E. Fleming, H.M. Solo-Gabriele, Shedding of *Staphylococcus aureus* and methicillin-resistant *Staphylococcus aureus* from adult and pediatric bathers in marine waters, BMC Microbiol. 11 (2011) 5.
[67] H.C. van der Mei, M. Rustema-Abbing, D.E. Langworthy, D.I. Collias, M.D. Mitchell, D.W. Bjorkquist, H.J. Busscher, Adhesion and viability of waterborne pathogens on P-DADMAC coatings, Biotechnol. Bioeng. 99 (2008) 165–169.
[68] W.C.E. Schofield, J.P.S. Badyal, A substrate-independent approach for bactericidal surfaces, ACS Appl. Mater. Interfaces 1 (2009) 2763–2767.
[69] M.R.J. Salton, Lytic agents, cell permeability, and monolayer penetrability, J. Gen. Physiol. 52 (1968) 227–252.
[70] B. Gottenbos, D.W. Grijpma, H.C. van der Mei, J. Feijen, H.J. Busscher, Antimicrobial effects of positively charged surfaces on adhering Gram-positive and Gram-negative bacteria, J. Antimicrob. Chemoth. 48 (2001) 7–13.
[71] S. Buffet-Bataillon, P. Tattevin, M. Bonnaure-Mallet, A. Jolivet-Gougeon, Emergence of resistance to antibacterial agents: the role of quaternary ammonium compounds–a critical review, Int. J. Antimicrob. Agents 39 (2012) 381–389.
[72] S. Bagherifard, D.J. Hickey, A.C. de Luca, V.N. Malheiro, A.E. Markaki, M. Guagliano, T.J. Webster, The influence of nanostructured features on bacterial adhesion and bone cell functions on severely shot peened 316L stainless steel, Biomaterials 73 (2015) 185–197.
[73] R. Sonohara, N. Muramatsu, H. Ohshima, T. Kondo, Difference in surface properties between *Escherichia coli* and *Staphylococcus aureus* as revealed by electrophoretic mobility measurements, Biophys. Chem. 55 (1995) 273–277.